

DEGENERACY BETWEEN LENSING AND OCCULTATION IN THE ANALYSIS OF SELF-LENSING PHENOMENA

CHEONGHO HAN

Department of Physics, Institute for Astrophysics, Chungbuk National University, 371-763 Cheongju, Republic of Korea
Draft version June 14, 2021

ABSTRACT

More than 40 years after the first discussion, it was recently reported the detection of a self-lensing phenomenon within a binary system where the brightness of a background star is magnified by its foreground companion. It is expected that the number of self-lensing binary detections will be increased in a wealth of data from current and future survey experiments. In this paper, we introduce a degeneracy in the interpretation of self-lensing light curves. The degeneracy is intrinsic to self-lensing binaries for which both magnification by lensing and de-magnification by occultation occur simultaneously and is caused by the difficulty in separating the contribution of the lensing-induced magnification from the observed light curve. We demonstrate the severity of the degeneracy by presenting example self-lensing light curves suffering from the degeneracy. We also present the relation between the lensing parameters of the degenerate solutions. The degeneracy would pose as an important obstacle in accurately determine self-lensing parameters and thus to characterize binaries.

Subject headings: gravitational lensing; micro – binaries; general

1. INTRODUCTION

Self lensing refers to the gravitational lensing phenomenon that occurs within a binary system where the brightness of a background star (source) is magnified by its foreground companion (lens). This concept was first mentioned by Trimble & Thorne (1969). Leibovitz & Hube (1971) and Maeder (1973) later pointed out that binary systems in which one member is a degenerate, compact object – a white dwarf (WD), neutron star (NS), or black hole (BH) – could cause repeated magnification of its companion star if the orbit happened to be viewed edge-on. The magnification of these self-lensing binary systems is very tiny, typically a part in one thousand or less for a Sun-like source star, and thus it was considered to be very difficult to detect such a phenomenon.

The concept of self lensing, which had been dormant for more than two decades, resurrected with the advent of new types of experiments that are equipped with instruments with greatly enhanced photometric precision and survey capability. With the start of Galactic microlensing surveys, Gould (1995) and later Rahvar et al. (2011) revisited self lensing and estimated the possibility of detecting self-lensing binaries in the data acquired from lensing surveys. Beskin & Tuntsov (2002) evaluated the prospect of detecting self-lensing binaries in the data obtained from Sloan Digital Sky Survey (SDSS). Kasuya et al. (2011) investigated lensing effects of a planet transiting its host star. Sahu & Gilliland (2003) and Farmer & Agol (2003) pointed out that space-based instruments such as *Kepler* and *Eddington* would be sensitive to compact objects in binaries through their microlensing signatures. Finally, by using *Kepler* data, Kruse & Agol (2014) reported the first discovery of a self-lensing binary system (KOI-3278) that is composed of a WD stellar remnant and a Sun-like companion. The number of self-lensing binary detections is expected to be increased in a wealth of data from current and future survey experiments.

Occultation and lensing are different limits of the same phenomena occurring when one body passes in front of another body (Agol 2002). Under some circumstances, both magnification of the source flux by lensing and de-magnification by occultation can simultaneously occur. This happens to bi-

naries composed of WD-star pairs for which the size of the lens (WD) is equivalent to the Einstein radius (Agol 2002; Marsh 2001). For example, the radius of the WD companion of KOI-3278 is $\sim 70\%$ of the estimated Einstein radius. Considering that WD-star pairs are important targets to observe self-lensing phenomena, there will be more self-lensing cases where both lensing and occultation are important.

In this paper, we introduce a degeneracy between lensing and occultation in the analysis of self-lensing phenomena. We demonstrate that this degeneracy is intrinsic and thus very severe, making it difficult to accurately characterize self-lensing binary systems.

The paper is organized as follows. In section 2, we describe basic physics of self lensing, including various effects that determines self-lensing light curves. In section 3, we introduce the degeneracy between lensing and occultation and demonstrate the severity of the degeneracy by presenting example self-lensing light curves suffering from the degeneracy. We summarize results and conclude in section 4.

2. BASIC PHYSICS OF SELF-LENSING

The basic difference between self-lensing and regular microlensing phenomena comes from the fact that the Einstein radius of the self-lensing phenomenon is much smaller than that of the regular lensing phenomenon. The Einstein radius is related to the mass of the lens, M_L , the distances to the lens, D_L , and source, D_S , by

$$r_E = \left(\frac{4GM_L}{c^2} \right)^{1/2} \left[\frac{D_L(D_S - D_L)}{D_S} \right]^{1/2}. \quad (1)$$

For self-lensing phenomena, $D_S \sim D_L \gg D_S - D_L \sim a$ and thus the second term within the brackets on the right side of equation (1) becomes $D_L(D_S - D_L)/D_S \sim a$, where a is the semi-major axis of the binary orbit. This term is much smaller than the factor $\sim D_L/2$ of the regular lensing phenomenon that occur by a lensing object located roughly halfway between the source and observer and thus Einstein radii of self-lensing phenomena are very small. To be also noted is that the Einstein radius of the self-lensing phenomenon does not depend

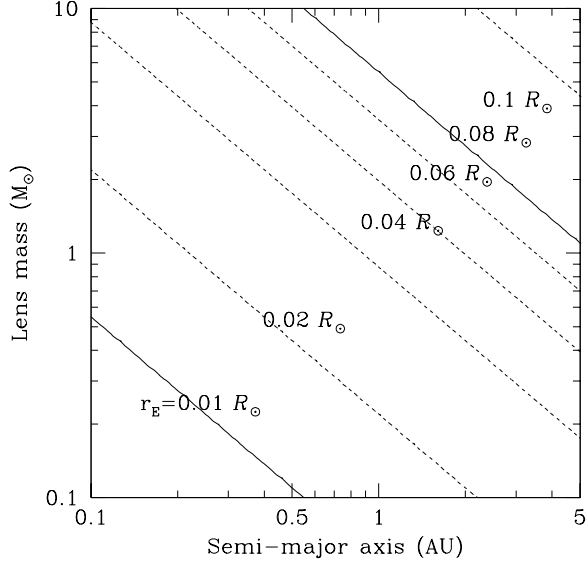


FIG. 1.— Einstein radii of self-lensing phenomena as a function of the semi-major axis of the binary and the mass of the lensing object.

on the distance to the binary (Maeder 1973), i.e.

$$r_E = \left(\frac{4GM_L a}{c^2} \right)^{1/2}. \quad (2)$$

Measuring the Einstein radius is important because it enables one to determine the physical parameters of the lens. In addition to the relation in equation (2), the mass and semi-major axis are related to each other by the Kepler's law

$$\frac{P^2}{a^3} = \frac{4\pi^2}{G(M_S + M_L)}. \quad (3)$$

Since the orbital period P and the mass of the lensed star M_S can be determined from follow-up photometric and spectroscopic observation, Kepler's law provides another relation between M_L and a . With the two unknowns and two relations, therefore, it is possible to determine the physical parameters of self-lensing binary systems.

In Figure 1, we present the Einstein radii of self-lensing phenomena as a function of the semi-major axis and the mass of a lensing object. For stellar-mass lensing objects with masses in the range $0.1 \lesssim M/M_\odot \lesssim 10$, the expected Einstein radii of self-lensing effects are in the range $0.01 \lesssim r_E/R_\odot \lesssim 0.1$ for binaries with semi-major axes $0.1 \lesssim a/\text{AU} \lesssim 5$. These Einstein radii are $\sim 10^3 - 10^4$ times smaller than the Einstein radii of Galactic microlensing events with typical radii of $r_E \sim (O) \text{ AU}$.

2.1. Magnification by Lensing

The most important consequence of very small Einstein radii of self-lensing phenomena is that lensing magnifications are affected by severe finite-source effects. Finite size of a source affects lensing magnifications due to a differential magnification, where different parts of the source surface are magnified by different amounts (Witt & Mao 1994). Finite-source effects are described by the ratio of the source radius r_* to the Einstein radius. For regular microlensing events, the ratio is $r_*/r_E \sim 10^{-3} - 10^{-2}$ and thus finite-source effects become important either for very rare cases of extremely high-magnification events, where the lens traverses or approaches

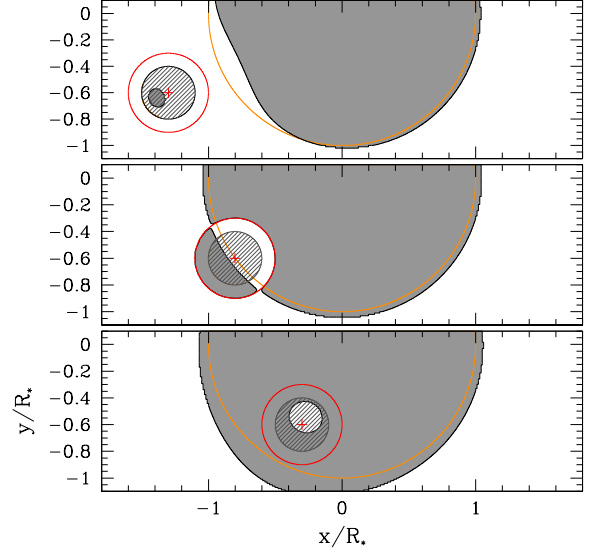


FIG. 2.— Variation of self-lensed images of a source with the change of the relative lens-source position. The orange circle and the grey shaded region represent the source and its lensed image, respectively. The lens is marked by a circle shaded by slanted lines and the “+” mark represents the center of the lens. The red circle around the lens represents the Einstein ring. The top and bottom panels show the images when the lens is out of and within the source surface, respectively. The middle panel shows the image at the moment of the lens entrance into the source surface.

very close to the source, or for events associated with extremely large source stars. On the other hand, the ratio is $r_*/r_E \sim 10^1 - 10^2$ for self-lensing phenomena that occur on typical main-sequence stars. As a result, self-lensing phenomena are always affected by severe finite-source effects and exhibit light curves that are very different from those of regular lensing events.

Under the assumption of a uniform disk, the lensing magnification of a finite source is computed as the area ratio of the lensed image to the source star. The image position, \mathbf{z} , for a given position of a source with respect to a lens, \mathbf{u} , is obtained by solving the lens equation

$$\mathbf{u} = \mathbf{z} - \mathbf{z}^{-1}, \quad (4)$$

where all lengths are normalized to the Einstein radius (Paczynski 1986; Witt & Mao 1994). Solving the equation with respect to \mathbf{z} yields two solutions of the image positions

$$\mathbf{z}_\pm = \frac{1}{2} \left[u \pm (u^2 + 4)^{1/2} \right] \frac{\mathbf{u}}{u}. \quad (5)$$

Figure 2 shows the variation of self-lensing images (grey shaded region) with the change of the lens (circle shaded by slanted lines) location with respect to the source (orange circle). We note that the positions of the image envelope are obtained by solving equation (5) for the positions along the envelope of the source. The center of the lens is marked by the “+” symbol and the Einstein radius around the lens is marked by a red circle. We note that a similar plot was presented in Figure 2 of Maeder (1973). When the lens is out of the source star surface ($u > r_*/r_E$), there exist two separate images: one big image located out of the Einstein ring (major image) and the other small image within the Einstein ring (minor image). On the other hand, when the lens is within the source star surface ($u < r_*/r_E$), there exists a single image with a small hole inside. The positions of the hole corresponds to those of the

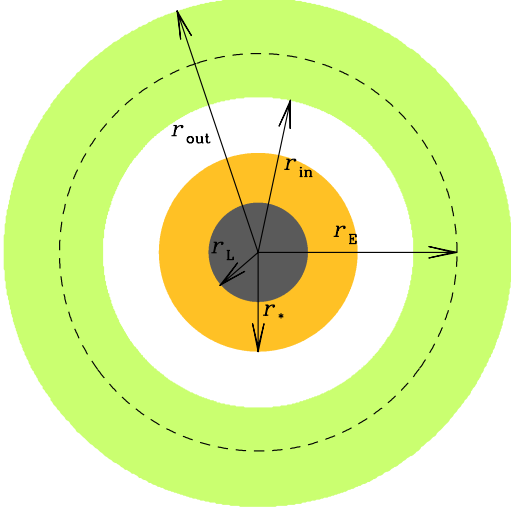


FIG. 3.— Geometry of a self-lensing system. The green annulus represents the image of a source when the source (yellow circle) is gravitational lensed by a lens (grey circle) that is exactly aligned with the source. The dashed circle is the Einstein ring.

minor image, i.e. \mathbf{z}_- in equation (5). Then, the magnification of a uniform, finite source is expressed as

$$A = \frac{\Sigma_I}{\Sigma_S} = \begin{cases} (\Sigma_{I,+} + \Sigma_{I,-})/\Sigma_S & \text{when } u > r_*/r_E, \\ (\Sigma_{I,+} - \Sigma_{I,-})/\Sigma_S & \text{when } u < r_*/r_E, \end{cases} \quad (6)$$

where $\Sigma_S = \pi r_*^2$ is the area of the source, and $\Sigma_{I,+}$ and $\Sigma_{I,-}$ are the areas of the major and minor images, respectively.

Under the assumption that the disk of a source is uniform, finite-source magnifications during very close lens-source approaches can be expressed in an analytic form. For the derivation of the analytic expression, we present the geometry of a self-lensing system in Figure 3. In the figure, the green annulus represents the image of a source when the source (yellow circle) is gravitational lensed by a lens (grey circle) that is exactly aligned with the source. The positions of the inner and outer circles of the image are the major- and minor-image locations corresponding to the envelope of the source, and thus the radii of the inner and outer circles are

$$\begin{aligned} r_{\text{in}} &= \frac{1}{2} \left[(r_*^2 + 4r_E^2)^{1/2} - r_* \right], \\ r_{\text{out}} &= \frac{1}{2} \left[(r_*^2 + 4r_E^2)^{1/2} + r_* \right], \end{aligned} \quad (7)$$

respectively. Then, the lensing magnification, which corresponds to area ratio of the image to the source, is expressed as (Maeder 1973; Riffeser et al. 2006)

$$A = \frac{r_{\text{out}}^2 - r_{\text{in}}^2}{r_*^2} = \left[1 + 4 \left(\frac{r_E}{r_*} \right)^2 \right]^{1/2}. \quad (8)$$

In the limiting case where $r_* \gg r_E$, equation (8) is approximated as¹ (Agol 2003)

$$A \sim 1 + 2 \left(\frac{r_E}{r_*} \right)^2. \quad (9)$$

¹ In other limiting cases, the finite magnification becomes $A = \sqrt{5}$ when $r_* = r_E$ and $A \sim 2r_E/r_*$ when $r_* \ll r_E$.

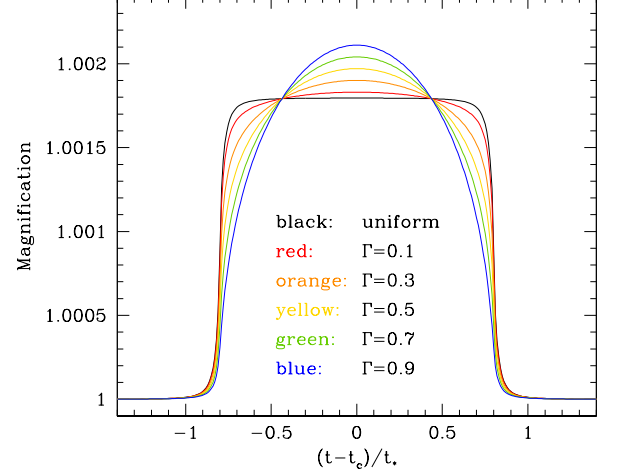


FIG. 4.— Variation of self-lensing light curves caused by limb-darkening effects. The adopted radii of the source and Einstein ring are $r_* = 1.0 R_\odot$ and $r_E = 0.03 R_\odot$, respectively. The definition of the limb-darkening coefficient Γ is provided in equation (10). The lens-source impact parameter is $0.6 r_*$. The notation t_* represents the time scale for the lens to cross the source radius and t_c represents the time of the lens approach to the center of the source.

This approximation is useful in estimating the peak magnifications of self-lensing events. For example, the peak magnifications with $r_E/r_* = 0.01, 0.05$, and 0.1 are $A_{\text{max}} = 1.0002, 1.005$, and 1.02 , respectively.

Stellar disks are not uniform in brightness. Instead, central part of a stellar disk appears brighter than the edge due to limb-darkening. Then, when finite-source effects are important in lensing magnifications, limb-darkening effects come along (Witt & Mao 1994). In Figure 4, we present the variation of lensing magnifications caused by limb-darkening effects. We model the surface brightness profile as (Yoo et al. 2004; Lee et al. 2009)

$$S_\lambda \propto 1 - \Gamma_\lambda \left(1 - \frac{3}{2} \cos \phi \right), \quad (10)$$

where Γ_λ is the linear limb-darkening coefficient and ϕ is the angle between the line of sight toward the center of the source star and the normal to the source surface. We note that Γ_λ depends not only on the stellar type of the source but also on the observed passband. We accommodate the limb-darkening effect on lensing light curves by dividing the source into multiple annuli and giving a weight of the surface brightness to each annulus in the computation of finite-source magnifications. We note that finite-source magnifications including limb darkening can also be computed by using analytic expressions derived by Witt & Mao (1994) for circular sources and Heyrovský & Loeb (1997) for elliptical sources. From the pattern of the variation, it is found that the limb-darkened magnification is higher than the magnification of a uniform disk when the lens is located at the center of the source star disk, where the surface brightness is high. In contrast, the magnification when the source is located at the edge, where the surface brightness is low, is lower than uniform-disk magnification. It is also found that the limb-darkening effect causes the flat top part of the light curve to appear rounder. These tendencies become more important as the limb-darkening coefficient increases.

2.2. De-magnification by Occultation

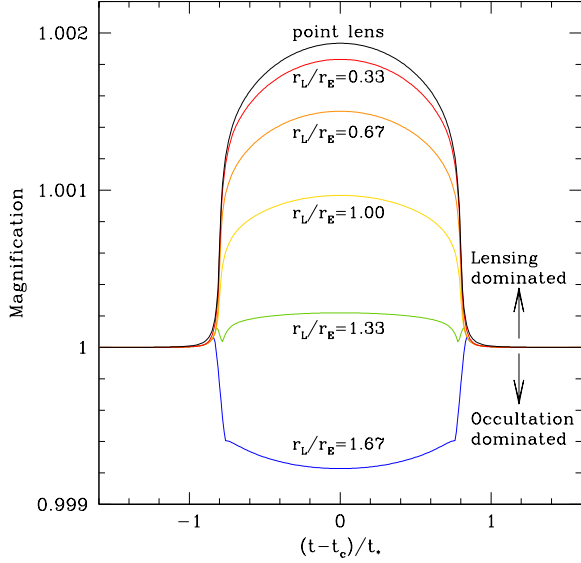


FIG. 5.— Variation of self-lensing light curves caused by occultation effects, which depend on ratios of the lens radius to the Einstein radius, r_L/r_E . The adopted source radius and the limb-darkening coefficient are $r_* = 1 R_\odot$ and $\Gamma = 0.4$, respectively. The lens-source impact parameter is $0.6r_*$. Notations are same as those in Figure 4.

Very small Einstein radii of self-lensing phenomena sometimes require to consider finite sizes of lenses. The effect of a finite lens on lensing magnification is caused because a lensed image can be partly blocked by the lens (Bromley 1996). The occultation of an image is illustrated in Figure 2. Since the blocked part of the image cannot be seen, finite-lens effects cause the lensing magnification to appear lower than the magnification of a point lens.

Occultation effects occur when the lens radius is greater than the inner radius of the image, i.e. $r_L > r_{in}$. Under this condition, lensing magnifications become (Agol 2003)

$$A = \frac{r_{out}^2 - r_L^2}{r_*^2} \sim 1 + 2 \left(\frac{r_E}{r_*} \right)^2 - \left(\frac{r_L}{r_*} \right)^2, \quad (11)$$

where the second term on the right side is the magnification term induced by lensing while the last term is the de-magnification term induced by finite-lens effects. Agol (2003) showed that the analytic expression holds when the lens is well inside the source. Then, the lensing magnification when the lens is located over the source star surface is expressed as

$$A \sim \begin{cases} 1 + 2(r_E/r_*)^2 & \text{when } r_L < r_{in}, \\ 1 + 2(r_E/r_*)^2 - (r_L/r_*)^2 & \text{when } r_{in} < r_L \leq r_{out}, \\ 0 & \text{when } r_L \geq r_{out}, \end{cases} \quad (12)$$

which is known as the “inverse-transit approximation” (Agol 2003; Marsh 2001). Note that $A = 0$ implies that the image is completely blocked out by the lens. We also note that the expression for exact lensing magnifications considering finite source and lens is provided by Lee et al. (2009).

De-magnification by occultation is important for self-lensing phenomenon where the radius of the lens is comparable to the Einstein radius, i.e. $r_E \sim r_L$ (Lee et al. 2009). For WD lenses, which are roughly the same size as the Earth, i.e. $r_L \sim 0.01 R_\odot$, the size of the lens can be a significant fraction of the Einstein radius and thus finite-lens effects can be important. For stellar lenses, on the other hand, the lens is much bigger than the Einstein radius, i.e. $r_L \gg r_E$. In this case, the

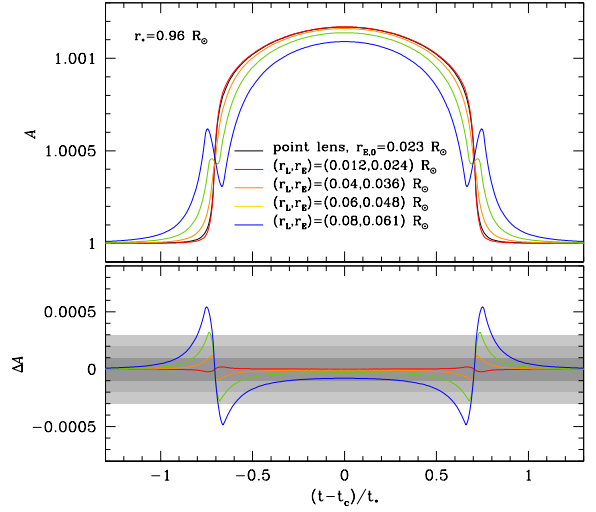


FIG. 6.— Self-lensing light curves with similar peak magnifications resulting from different combinations of the Einstein ring radius r_E and lens radius r_L . The lower panel shows the residual from the point-lens light curve. The shaded regions with different grey tones represent the 1σ , 2σ , and 3σ photometric precisions of *Kepler* observation achieved in 15 min sampling for a $V = 12$ star.

resulting light curve of the background star is simply that of an eclipsing binary where lensing signatures cannot be detected.

In Figure 5, we present light curves of self-lensing events with different ratios of the lens radius to the Einstein radius. From the comparison of the light curves, it is found that magnifying lensing effects and de-magnifying occultation effects compete each other depending on the ratio r_L/r_E . For small r_L/r_E ratios, lensing effects dominate and the source flux is magnified. As the ratio increases, occultation effects become more important.

3. DEGENERACY

The simultaneous occurrence of magnification by lensing and de-magnification by occultation provokes a question on whether the contribution of the lensing-induced magnification can be separated from observed light curves in order to accurately determine the Einstein radius and thus to characterize binary systems. To answer the question, we compare self-lensing light curves with similar peak magnifications but with different combinations of the Einstein ring and the lens radii. For a given magnification and a source radius, the relation between r_E and r_L of degenerate solutions are obtained from equation (12), i.e.

$$r_E^2 = \frac{1}{2} [r_L^2 + (A - 1)r_*^2]. \quad (13)$$

We note that this expression is valid for $r_{in} < r_L \leq r_{out}$.

Figure 6 shows example degenerate light curves resulting from 5 different combinations of r_E and r_L . The lensing parameters are chosen so that the individual light curves can explain the observed light curve of the self-lensing binary KOI-3278. We note that the model parameters presented by Kruse & Agol (2014) are $r_* = 0.96 R_\odot$, $r_L = 0.012 R_\odot$, and $r_E = 0.024 R_\odot$ and the lens-source impact parameter is $0.706 r_*$. The lower panel shows the residuals from the point-lens case, i.e. $r_L = 0$. We note that for all degenerate cases, the lens radius is significantly larger than the inner radius of the image r_{in} . In Figure 7, we also present the distribution of the fractional deviation of the peak magnification $A_{max,FL}$

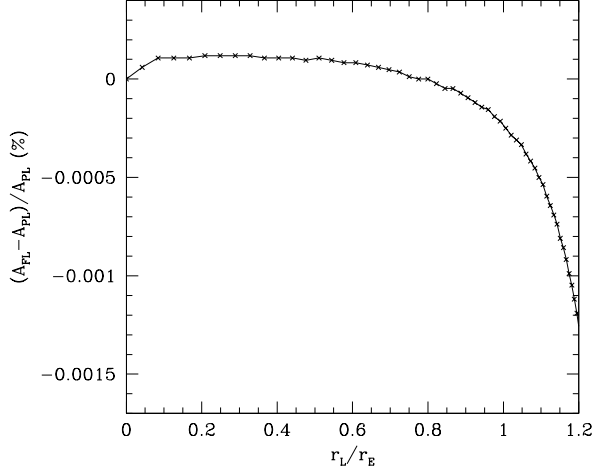


FIG. 7.— Fractional deviation of the peak magnification affected by finite lens effects, $A_{\max,FL}$, from the point-lens magnification, $A_{\max,PL}$, as a function of the lens to Einstein radius ratio, r_L/r_E .

from the point-lens magnification $A_{\max,PL}$ as a function of the lens to Einstein radius ratio, r_L/r_E .

From the comparison of the light curves, it is found that the light curves are similar each other despite the large differences in the values of r_E and r_L . The degeneracy between light curves is especially severe when the lens is smaller than the Einstein ring. It is found that the difference in the fractional magnification is $\Delta A/A \lesssim 0.5 \times 10^{-4}$ for self-lensing

events with $r_L \lesssim r_E$. The photometric precision of *Kepler* is $\sim 100 \mu\text{mag}$, 1σ error achieved in 15 min sampling for a $V = 12$ star (Argabright et al. 2008; Van Cleve & Caldwell 2009), which corresponds to $\Delta A/A \sim 10^{-4}$. Then, although self-lensing itself, with $\Delta A/A \sim 20 \times 10^{-4}$, can be detected with a significant statistical confidence, it will be difficult to distinguish degenerate light curves suffering from the lensing/occultation degeneracy.

With the increase of r_L/r_E ratio, the deviation from the point-lens light curve increases. It is found that the major deviations occur during the ingress and egress of the lens over the source surface. Considering the photometric precision of *Kepler*, however, it is expected that resolving the degeneracy will be possible for only events that experience severe occultation effects.

4. SUMMARY

We introduced a degeneracy that would happen in interpreting light curves of self-lensing phenomena. We found that the degeneracy was intrinsic to self-lensing binaries for which both magnification by lensing and de-magnification by occultation occur simultaneously. We found that the degeneracy was severe and would be difficult to resolve by the precision of *Kepler* data. Therefore, the degeneracy would pose as an important obstacle in accurately determine self-lensing parameters and thus to characterize binaries.

This Work was supported by Creative Research Initiative Program (2009-0081561) of National Research Foundation of Korea. We thank A. Gould for making useful comments.

REFERENCES

- Agol, E. 2002, *ApJ*, 579, 430
 Agol, E. 2003, *ApJ*, 594, 449
 Argabright, V. S., VanCleve, J. E., Bachtell, E. E., et al. 2008, *Proc. SPIE*, 7010, 70102L
 Beskin, G. M., & Tuntsov, A. V. 2002, *A&A*, 394, 489
 Bromley, B. C. 1996, *ApJ*, 467, 537
 Dominik, M. 1998, *A&A*, 333, L79
 Gould, A. 1995, *ApJ*, 441, 77
 Gould, A., & Gaucherel, C. 1997, *ApJ*, 477, 580
 Farmer, A. J., & Agol, E. 2003, *ApJ*, 592, 1151
 Hambly, N. C., Smartt, S. J., & Hodgkin, S. T. 1997, *ApJ*, 489, L157
 Heyrovský, D., & Loeb, A. 1997, *ApJ*, 490, 38
 Kasuya, S., Honda, M., & Mishima, R. 2011, *MNRAS*, 411, 1863
 Kruse, E., & Agol, E. 2014, *Science*, 344, 275
 Leibovitz, C., & Hube, D. P. 1971, *A&A*, 15, 251
 Lee, C.-H., Riffeser, A., Seitz, S., & Bender, R. 2009, *ApJ*, 695, L200
 McCook, G. P., & Sion, E. M. 1999, *ApJS*, 121, 1
 Maeder, A. 1973, *A&A*, 26, 215
 Marsh, T. R. 2001, *MNRAS*, 324, 547
 Paczyński, B. 1986, *ApJ*, 304, 1
 Rahvar, S., Mehrabi, A., & Dominik, M. 2011, *MNRAS*, 410, 912
 Riffeser, A., Fliri, J., Seitz, S., & Bender, R. 2006, *ApJS*, 163, 225
 Sahu, K. C., & Gilliland, R. 2003, *ApJ*, 584, 1042
 Trimble, V. L., & Thorne, K. S. 1969, *ApJ*, 156, 1013
 Van Cleve, J., & Caldwell, D. A. 2009, *Kepler Instrument Handbook*, KSCI 19033-001 (Moffett Field, CA: NASA Ames Research Center), <http://archive.stsci.edu/kepler/>
 Witt, H. J., & Mao, S. 1994, *ApJ*, 430, 505
 Yoo, J., DePoy, D. L., Gal-Yam, A., et al. 2004, *ApJ*, 603, 139